JASA ARTICLE

Block-sparse two-dimensional off-grid beamforming with arbitrary planar array geometry

Yongsung Park,[1,a)] Woojae Seong,[2,b)] and Peter Gerstoft[1,c)]
[1]*Scripps Institution of Oceanography, University of California San Diego, La Jolla, California 92093-0238, USA*
[2]*Department of Naval Architecture and Ocean Engineering and Research Institute of Marine System Engineering, Seoul National University, Seoul 08826, South Korea*

ABSTRACT:
For a sound field observed on a planar sensor array, compressive sensing (CS) reconstructs the two-dimensional (2D) direction-of-arrival (DOA) of multiple sources using a sparsity constraint. Conventional compressive beamforming methods suffer from grid mismatch, where true DOAs do not fall on the discretized angular search grid. This paper adopts a CS-based model, which can reconstruct block-sparse signals, and the model treats DOAs and the off-grid DOA compensation parts as blocks to deal with the off-grid 2D beamforming. The method is illustrated by numerical simulations and shows high estimation accuracy. Also, the approach does not require a specific array configuration and is suitable for arbitrary planar array geometry, which is practically useful. Since propeller tip vortex cavitation induces noise sources located sparsely near the propeller tip, the high-resolution of the method is demonstrated with experimental data from cavitation tunnel experiments. © *2020 Acoustical Society of America*.
https://doi.org/10.1121/10.0000983
(Received 13 December 2019; revised 2 March 2020; accepted 12 March 2020; published online 6 April 2020)
[Editor: Jianlong Li] Pages: 2184–2191

I. INTRODUCTION

Direction-of-arrival (DOA) estimation refers to the process of estimating directions of several sources from measurements of the wave-field with sensors that form an array. We consider the case of estimating the two-dimensional (2D) DOAs, azimuth, and elevation of the radiated sources incident on a planar array. Compressive beamforming [compressive sensing (CS)[1] based DOA estimation] shows high-resolution DOA estimation performance using a sparsity constraint, and 2D planar array geometry enables the compressive beamforming[2–4] to deal with the 2D beamforming. We propose compressive 2D off-grid beamforming for estimating 2D DOAs of multiple sources, where the off-grid model mitigates the grid mismatch that deteriorates the DOA estimation performance of classical compressive beamforming models, which uses discretized angular search grid. Another important practical feature is that the presented model is not limited to a specific array geometry and is applicable to arbitrary planar array geometry.

CS efficiently solves a sparse signal reconstruction problem[5] and has been used in various applications for parameter estimation.[6–12] Compressive beamforming has proved to provide good DOA estimation performance.[2–4,13,14] Classical compressive beamforming employs a discretized angular grid for DOA estimation, and the mismatch between the true DOAs and the discrete angular grid deteriorates the estimation performance, which is basis mismatch.[15,16] To overcome the basis mismatch, off-grid compressive beamforming[17] and grid-free (gridless) compressive beamforming[15,16] are suggested.

Two or three-dimensional array configuration allows estimating 2D DOAs (2D beamforming),[18,19] and compressive 2D beamforming has been presented.[20–22] Compressive 2D beamforming with classical CS also suffers from the basis mismatch. Thus, the off-grid or the grid-free technique can be a remedy. For compressive 2D beamforming with grid-free CS, grid-free CS for multi-dimensional parameter estimation[23,24] was employed.[25] However, it is limited to a uniform rectangular array configuration case in its mathematical framework, and the suggested non-uniform array cannot cover an arbitrary array configuration. Meanwhile, off-grid CS[17] utilizes a discretized parameter-search grid and offsets the difference between grid and off-grid true DOA using first-order Taylor expansion around the grid. The off-grid CS has been employed in 2D off-grid beamforming.[26,27] However, two offset terms in azimuth and elevation have been treated separately into two 1 D beamforming problems, and these methods are suitable only for specific array configurations.

This paper proposes a compressive 2D off-grid beamforming method. Inspired by the off-grid CS,[17] compensation for the off-grid DOAs in azimuth and elevation is considered for an off-grid model, and three terms, which include a discretized angular grid and two offset terms for off-grid azimuth and off-grid elevation, should be processed jointly. The three terms share the same angular grid and group in the concept of a block. The compressive 2D off-grid beamforming is interpreted in a block-sparse signal

[a)]Electronic mail: yongsungpark@ucsd.edu, ORCID: 0000-0001-6692-0262.
[b)]ORCID: 0000-0002-5393-7097.
[c)]ORCID: 0000-0002-0471-062X.

https://doi.org/10.1121/10.0000983

reconstruction problem and solved by CS for block-sparse signals,[28,29] called "block-sparse CS" here.

The suggested method has no array geometry limitation; the system framework is based on the conventional beamforming[30] and its derivatives. From an algorithmic point of view, the block-sparse CS is a mixed l_2/l_1-norm minimization,[28] which is solved efficiently without using any information related to array geometry.

To demonstrate the high-resolution beamforming capabilities and the applicability of the method to arbitrary array geometry, the presented method is applied to underwater acoustic measurements for propeller tip vortex cavitation (TVC) noise source tracking. To explore the characteristics of propeller cavitation noise, cavitation tunnel experiments have been conducted,[31–34] and the propeller cavitation localization has been studied,[35–37] including TVC noise localization.[38–40] Given that TVC noise is sparse near the top center (upper downstream area or top to starboard direction) of the propeller and each source acts like a monopole, CS methodology was used.[40] Beamforming is used to localize the propeller TVC noise,[39] and sparse representation of the TVC noise can be used for compressive 2D beamforming.

Another feature of the cavitation noise measurement experiments is that various array configurations are employed,[35,39] and even acoustic sensors are attached to the hull of a ship.[36,38] The suggested scheme does not require a specific array configuration, thus experimental data applications can benefit from the arbitrary array applicability.

The key features of the proposed method are as follows: CS-based 2D beamforming technique localizes azimuth and elevation of multiple sources, off-grid beamforming capability is achieved via block-sparse CS, and the presented scheme allows arbitrary array configuration applications.

II. ARRAY DATA MODEL AND PROBLEM FORMULATION

Consider K narrowband far-field sources s_k, $k = 1, \ldots, K$, arriving at an array of M sensors from DOAs (θ_k, ϕ_k), $k = 1, \ldots, K$. Here, the vertical angle θ in elevation is defined as the angle from the positive z-axis to the line of view, and the horizontal angle ϕ in azimuth is defined as the angle from the positive x axis to the projection of the line of view on the horizontal plane (see Fig. 1). The measurement $\mathbf{y} \in \mathbb{C}^M$ is modeled as

$$y_m = \sum_{k=1}^{K} a_m(\theta_k, \phi_k) s_k + e_m, \quad m = 1, \ldots, M, \tag{1}$$

where $\mathbf{y} = [y_1, \ldots, y_M]^{\mathsf{T}}$ is the vector of recorded measurements at the M sensors; $\mathbf{s} = [s_1, \ldots, s_K]^{\mathsf{T}} \in \mathbb{C}^K$ is the vector of K source amplitudes; $a_m(\theta_k, \phi_k)$ contains DOA of the kth source on the array and has phase delay information of the kth source to the mth sensor in its phase; $(\boldsymbol{\theta}, \boldsymbol{\phi}) = \{(\theta_1, \phi_1), \ldots, (\theta_K, \phi_K)\}$ is a set with K elements whose elements (θ_k, ϕ_k) are kth source vertical angles θ_k and horizontal angles ϕ_k, $k = 1, \ldots, K$; and $\mathbf{e} = [e_1, \ldots, e_M]^{\mathsf{T}} \in \mathbb{C}^M$

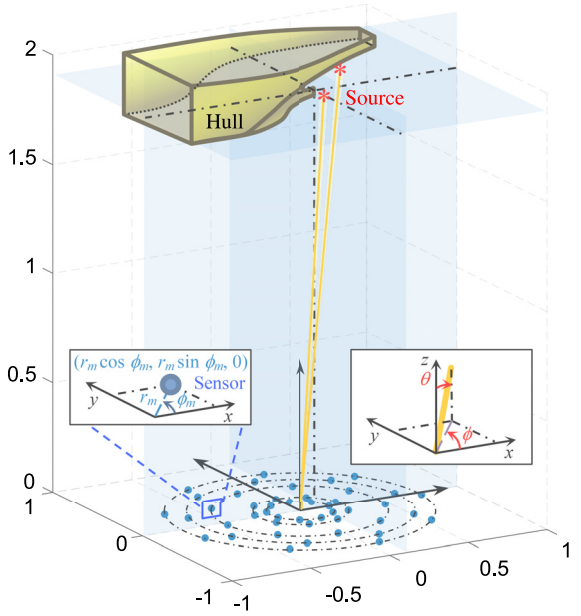

FIG. 1. (Color online) Configuration of the cavitation tunnel experiment with a 45-channel hydrophone array.

is the vector of measurement noise at the M sensors. The measurement vector of the sensor array is

$$\mathbf{y} = \mathbf{A}\mathbf{s} + \mathbf{e}, \tag{2}$$

where $\mathbf{A}(\boldsymbol{\theta}, \boldsymbol{\phi}) = [\mathbf{a}(\theta_1, \phi_1), \ldots, \mathbf{a}(\theta_K, \phi_K)] \in \mathbb{C}^{M \times K}$ is an array manifold matrix.

We are concerned with a 2D planar array, as shown in Fig. 1. Let the mth sensor position $(p_{x,m}, p_{y,m}, p_{z,m}) = (r_m \cos\phi_m, r_m \sin\phi_m, 0)$, $m = 1, \ldots, M$. The steering vector of the kth source $\mathbf{a}(\theta_k, \phi_k) \in \mathbb{C}^M$ is

$$\mathbf{a}(\theta_k, \phi_k) = \left[e^{j(2\pi/\lambda)(p_{x,1} \sin\theta_k \cos\phi_k + p_{y,1} \sin\theta_k \sin\phi_k)}, \ldots, e^{j(2\pi/\lambda)(p_{x,M} \sin\theta_k \cos\phi_k + p_{y,M} \sin\theta_k \sin\phi_k)}\right]^{\mathsf{T}}, \tag{3}$$

where λ is the signal wavelength. Using Cartesian coordinates with the unit vectors in the direction of the x, y, and z, $(u_k, v_k, w_k) = (\sin\theta_k \cos\phi_k, \sin\theta_k \sin\phi_k, \cos\theta_k)$, $k = 1, \ldots, K$, the elements of the steering vector in Eq. (3) becomes

$$\mathbf{a}(u_k, v_k) = \left[e^{j(2\pi/\lambda)(p_{x,1}u_k + p_{y,1}v_k)}, \ldots, e^{j(2\pi/\lambda)(p_{x,M}u_k + p_{y,M}v_k)}\right]^{\mathsf{T}}. \tag{4}$$

Let $\tilde{\boldsymbol{\theta}} = \{\tilde{\theta}_1, \ldots, \tilde{\theta}_{N_\theta}\} \in [-90°, 90°)$ be a discretized angular search-grid by N_θ vertical angles and $\tilde{\boldsymbol{\phi}} = \{\tilde{\phi}_1, \ldots, \tilde{\phi}_{N_\phi}\} \in [0°, 180°)$ be a discretized angular search-grid by N_ϕ horizontal angles. The search-grid in the u-v space, characterized by $\tilde{\boldsymbol{\theta}}$ and $\tilde{\boldsymbol{\phi}}$, is $\tilde{\boldsymbol{\Omega}} = \{(\tilde{u}_n, \tilde{v}_n)\}$, $n = 1, \ldots, N (= N_\theta \times N_\phi)$.

Suppose $(u_k, v_k) \notin \tilde{\boldsymbol{\Omega}} = \{(\tilde{u}_1, \tilde{v}_1), \ldots, (\tilde{u}_N, \tilde{v}_N)\}$ for some $k \in \{1, \ldots, K\}$ and that $(\tilde{u}_{n_k}, \tilde{v}_{n_k}) \in \tilde{\boldsymbol{\Omega}}$ is the nearest grid point to (u_k, v_k), $n_k \in \{1, \ldots, N\}$. For an off-grid DOA position,

$$u_k = \tilde{u}_{n_k} + \delta\tilde{u}_{n_k},$$
$$v_k = \tilde{v}_{n_k} + \delta\tilde{v}_{n_k}, \tag{5}$$

where $\delta\tilde{u}_{n_k}$ and $\delta\tilde{v}_{n_k}$ are off-grid differences in u and v, we approximate the steering vector for the off-grid DOAs $\mathbf{a}(u_k, v_k)$ using the first-order Taylor expansion,[17]

$$\begin{aligned}\mathbf{a}(u_k, v_k) &= \mathbf{a}(\tilde{u}_{n_k} + \delta\tilde{u}_{n_k}, \tilde{v}_{n_k} + \delta\tilde{v}_{n_k}) \\ &\approx \mathbf{a}(\tilde{u}_{n_k}, \tilde{v}_{n_k}) + \mathbf{a}_u(\tilde{u}_{n_k}, \tilde{v}_{n_k})\delta\tilde{u}_{n_k} \\ &\quad + \mathbf{a}_v(\tilde{u}_{n_k}, \tilde{v}_{n_k})\delta\tilde{v}_{n_k},\end{aligned} \tag{6}$$

where

$$\begin{aligned}\mathbf{a}_u(\tilde{u}_n, \tilde{v}_n) &= \left.\frac{\partial \mathbf{a}(u,v)}{\partial u}\right|_{(\tilde{u}_n, \tilde{v}_n)} \\ &= \left[\frac{j2\pi p_{x,1}\tilde{u}_n}{\lambda} e^{j(2\pi/\lambda)(p_{x,1}\tilde{u}_n + p_{y,1}\tilde{v}_n)}, \ldots, \right. \\ &\quad \left. \frac{j2\pi p_{x,M}\tilde{u}_n}{\lambda} e^{j(2\pi/\lambda)(p_{x,M}\tilde{u}_n + p_{y,M}\tilde{v}_n)}\right]^{\mathsf{T}}, \\ \mathbf{a}_v(\tilde{u}_n, \tilde{v}_n) &= \left.\frac{\partial \mathbf{a}(u,v)}{\partial v}\right|_{(\tilde{u}_n, \tilde{v}_n)} \\ &= \left[\frac{j2\pi p_{y,1}\tilde{v}_n}{\lambda} e^{j(2\pi/\lambda)(p_{x,1}\tilde{u}_n + p_{y,1}\tilde{v}_n)}, \ldots, \right. \\ &\quad \left. \frac{j2\pi p_{y,M}\tilde{v}_n}{\lambda} e^{j(2\pi/\lambda)(p_{x,M}\tilde{u}_n + p_{y,M}\tilde{v}_n)}\right]^{\mathsf{T}},\end{aligned} \tag{7}$$

for $n = 1, \ldots, N$ and $n_k \in \{1, \ldots, N\}$. Denote

$$\mathbf{A}_1 = [\mathbf{a}(\tilde{u}_1, \tilde{v}_1), \ldots, \mathbf{a}(\tilde{u}_N, \tilde{v}_N)] \in \mathbb{C}^{M\times N}, \tag{8a}$$
$$\mathbf{A}_2 = [\mathbf{a}_u(\tilde{u}_1, \tilde{v}_1), \ldots, \mathbf{a}_u(\tilde{u}_N, \tilde{v}_N)] \in \mathbb{C}^{M\times N}, \tag{8b}$$
$$\mathbf{A}_3 = [\mathbf{a}_v(\tilde{u}_1, \tilde{v}_1), \ldots, \mathbf{a}_v(\tilde{u}_N, \tilde{v}_N)] \in \mathbb{C}^{M\times N}. \tag{8c}$$

Note that matrices $\{\mathbf{A}_1, \mathbf{A}_2, \mathbf{A}_3\}$ have $N(= N_\theta \times N_\phi)$ columns. Reordering columns of $[\mathbf{A}_1, \mathbf{A}_2, \mathbf{A}_3] \in \mathbb{C}^{M\times 3N}$ with respect to $(\tilde{u}_n, \tilde{v}_n)$, we can represent $\tilde{\mathbf{A}}$ as a concatenation of column-blocks $\tilde{\mathbf{A}}[n]$ of size $M \times 3$,

$$\begin{aligned}\tilde{\mathbf{A}} = \Big[&\underbrace{\mathbf{a}(\tilde{u}_1, \tilde{v}_1), \mathbf{a}_u(\tilde{u}_1, \tilde{v}_1), \mathbf{a}_v(\tilde{u}_1, \tilde{v}_1)}_{\tilde{\mathbf{A}}[1]}, \\ &\underbrace{\mathbf{a}(\tilde{u}_2, \tilde{v}_2), \mathbf{a}_u(\tilde{u}_2, \tilde{v}_2), \mathbf{a}_v(\tilde{u}_2, \tilde{v}_2)}_{\tilde{\mathbf{A}}[2]}, \\ &\ldots, \underbrace{\mathbf{a}(\tilde{u}_N, \tilde{v}_N), \mathbf{a}_u(\tilde{u}_N, \tilde{v}_N), \mathbf{a}_v(\tilde{u}_N, \tilde{v}_N)}_{\tilde{\mathbf{A}}[N]}\Big].\end{aligned} \tag{9}$$

Absorbing the approximation error $\mathbf{e}^o$ in Eq. (6) into the measurement noise $\mathbf{e}$, $\tilde{\mathbf{e}} = \mathbf{e} + \mathbf{e}^o$, the measurement model in Eq. (2) becomes

$$\mathbf{y} = \mathbf{A}\mathbf{s} + \mathbf{e} = \tilde{\mathbf{A}}\mathbf{x} + \mathbf{e}^o + \mathbf{e} = \tilde{\mathbf{A}}\mathbf{x} + \tilde{\mathbf{e}}, \tag{10}$$

where we view $\mathbf{x} \in \mathbb{C}^{3N}$ as a concatenation of N blocks with $\mathbf{x}[n]$ denoting the nth block,

$$\mathbf{x} = [\underbrace{x_1, x_2, x_3}_{\mathbf{x}^{\mathsf{T}}[1]}, \underbrace{x_4, x_5, x_6}_{\mathbf{x}^{\mathsf{T}}[2]}, \ldots \underbrace{x_{3N-2}, x_{3N-1}, x_{3N}}_{\mathbf{x}^{\mathsf{T}}[N]}]^{\mathsf{T}} \tag{11}$$

for $n = 1, \ldots, N$. By considering $\mathbf{x}$ as a concatenation of blocks, we expect that $\mathbf{x}$ has nonzero entries appearing in blocks, i.e.,

$$\mathbf{x}^{\mathsf{T}}[n] = \begin{cases} s_k[1, \delta\tilde{u}_{n_k}, \delta\tilde{v}_{n_k}], & \text{if } n = n_k \\ & \text{for any } k \in \{1, \ldots, K\}, \\ 0, & \text{otherwise.}\end{cases} \tag{12}$$

The recovery of block-sparse vector $\mathbf{x}$ from measurements $\mathbf{y}$ in Eq. (10) is the off-grid model of focus in this paper. Note that, from $\mathbf{x}[n]$, s_k, $\delta\tilde{u}_{n_k}$, and $\delta\tilde{v}_{n_k}$ are obtained. Hereby $u_k = \tilde{u}_{n_k} + \delta\tilde{u}_{n_k}$ and $v_k = \tilde{v}_{n_k} + \delta\tilde{v}_{n_k}$ are obtained. From $u_k = \sin\theta_k \cos\phi_k$ and $v_k = \sin\theta_k \sin\phi_k$, $k = 1, \ldots, K$, resultant θ_k and ϕ_k are estimated.

III. 2D OFF-GRID BEAMFORMING WITH BLOCK-SPARSE CS

The problem of 2D DOA estimation is to recover the source vector $\mathbf{x} \in \mathbb{C}^N$, given the sensing matrix formed by the steering vectors at all angular search grid $\mathbf{A}_1 \in \mathbb{C}^{M\times N}$ in Eq. (8a) and an observation vector $\mathbf{y} \in \mathbb{C}^M$.

Conventional beamforming (CBF)[30] is the simplest DOA estimator based on the l_2-norm minimization method and yields the estimate

$$\mathbf{x}_{\text{CBF}} = \mathbf{A}_1^{\mathsf{H}}\mathbf{y}. \tag{13}$$

CBF is applicable to single snapshot measurements and robust to the noise, but suffers from low resolution and the presence of high-level sidelobes.

Using sparsity of the source vector $\mathbf{x} \in \mathbb{C}^N$ when the number of sources $K \ll N$, CS-based DOA estimation techniques can be used. Compressive beamforming based on the l_1-norm minimization problem is given by[2]

$$\min_{\mathbf{x}\in\mathbb{C}^N} \|\mathbf{x}\|_1 \quad \text{s.t. } \|\mathbf{y} - \mathbf{A}_1\mathbf{x}\|_2 \le \epsilon^{(l_1)}, \tag{14}$$

where $\epsilon^{(l_1)}$ is the noise floor.[2–4] We refer to Eq. (14) as "conventional CS."

2D off-grid DOA estimation is used to recover the source vector, including off-grid differences in Eq. (5), $\mathbf{x} \in \mathbb{C}^{3N}$, given the sensing matrix $\tilde{\mathbf{A}} \in \mathbb{C}^{M\times 3N}$ in Eq. (9) and an observation vector $\mathbf{y} \in \mathbb{C}^M$ in Eq. (10).

As addressed in Ref. 28, $\mathbf{x}$ in Eq. (11) is "block K-sparse" if $\mathbf{x}[n]$ has a nonzero Euclidean norm for at most K indices n and the Euclidean norm of the nth block is defined as

$$x_n^{(l_2)} = \|\mathbf{x}[n]\|_2 = \sqrt{x_{3n-2}^2 + x_{3n-1}^2 + x_{3n}^2} \tag{15}$$

for $n = 1, \ldots, N$. "Block-sparsity," the number of nonzero blocks, is defined as $\sum_{n=1}^N I(x_n^{(l_2)} > 0)$, where $I(\cdot)$ is the indicator function. Minimizing the block-sparsity promotes

https://doi.org/10.1121/10.0000983

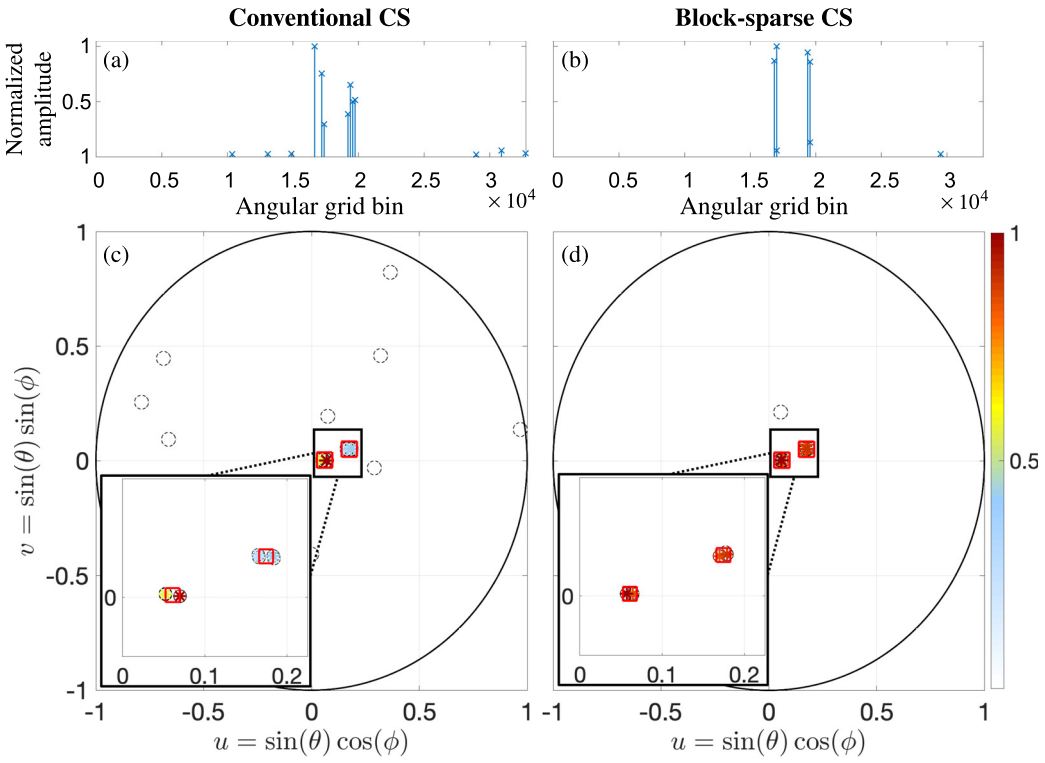

FIG. 2. (Color online) Activate components of sparse solution $\mathbf{x}$ in 2D beamforming using (a) conventional CS and (b) block-sparse CS. There are two equal strength sources under SNR = 20 dB. Same noise floor ($\epsilon = \epsilon^{(l_1)} = \|\mathbf{e}\|_2$) is used. 2D angular grid bin indicates grid points in $\tilde{\mathbf{\Omega}} = \{(\tilde{u}_n, \tilde{v}_n)\}$, $n = 1, \ldots, N(= N_\theta \times N_\phi = 181 \times 181 = 32761)$. The corresponding beamforming with (c) conventional CS and (d) block-sparse CS. Each panel is normalized by its peak value and plotted in power (linear).

sparse solutions, of which nonzero blocks give the source amplitudes and off-grid differences. The corresponding minimization problem to obtain a block-sparse solution $\mathbf{x}$ is given by[28]

$$\min_{\mathbf{x}\in\mathbb{C}^{3N}} \sum_{n=1}^{N} I(x_n^{(l_2)} > 0) \quad \text{s.t. } \|\mathbf{y} - \tilde{\mathbf{A}}\mathbf{x}\|_2 \le \epsilon, \tag{16}$$

where ϵ is the noise floor, i.e., $\|\tilde{\mathbf{e}}\|_2 \le \epsilon$. Unfortunately, solving Eq. (16) itself, pursuing every combination of nonzero blocks, is in general an NP-hard problem. Relaxation of the minimization in Eq. (16) to the closest convex optimization problem can be cast; then, the minimization problem is given by[28]

$$\min_{\mathbf{x}\in\mathbb{C}^{3N}} \|\mathbf{x}^{(l_2)}\|_1 \quad \text{s.t. } \|\mathbf{y} - \tilde{\mathbf{A}}\mathbf{x}\|_2 \le \epsilon, \tag{17}$$

where $\mathbf{x}^{(l_2)} = [x_1^{(l_2)}, \ldots, x_N^{(l_2)}]$. The optimization of Eq. (17) is performed over $\mathbf{x}$; $\mathbf{x}^{(l_2)}$ is a function of $\mathbf{x}$. We refer to Eq. (17) as "block-sparse CS." Note that for $x_{3n-1} = x_{3n} = 0$, $n = 1, \ldots, N$, the block-sparse CS in Eq. (17) is identical to the conventional CS in Eq. (14). Herein, we use the CVX program[41] (available in MATLAB) to solve the conventional CS in Eq. (14) and the block-sparse CS in Eq. (17).

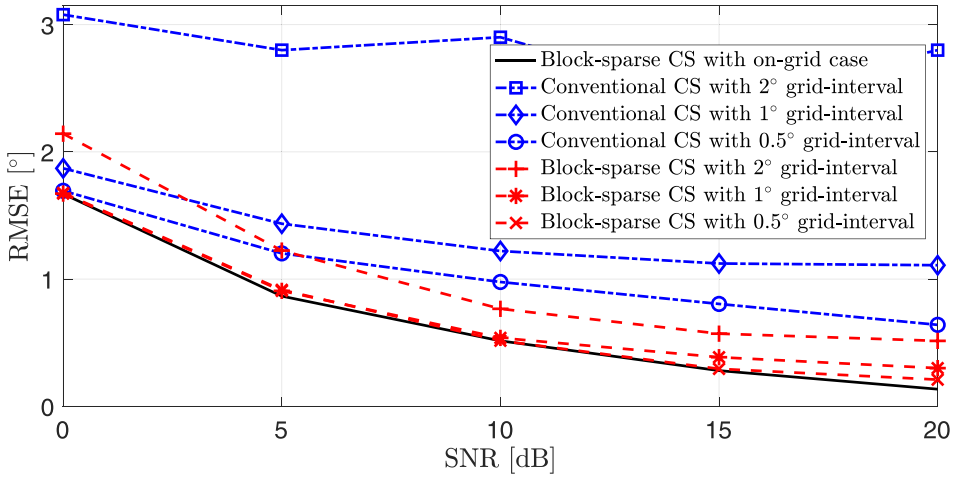

FIG. 3. (Color online) RMSE (°) comparison between conventional CS and block-sparse CS based 2D beamforming. Each RMSE is averaged over 100 trials.

IV. SIMULATION RESULTS

The block-sparse CS performance in 2D off-grid beamforming is evaluated through simulations and compared with conventional CS. The array of sensors is configured with 5 concentric circles of which the radii range from 0.18 to 0.75 m. Each circle consists of 9 hydrophones uniformly separated on the circle. The array configuration is followed by that of the cavitation tunnel experiment in Ref. 39.

The 2D off-grid beamforming capability is achieved with the compensation terms for off-grid DOAs, $\mathbf{A}_2$ and $\mathbf{A}_3$ in Eq. (8). We consider $K=2$ equal strength sources at $(\boldsymbol{\theta},\boldsymbol{\phi}) = \{(3.5^\circ, 2.5^\circ), (11.5^\circ, 16.5^\circ)\}$ with frequency $f=30$ kHz. The angular search grid is set on searching $\tilde{\boldsymbol{\theta}} = [-90 : 1 : 90]^\circ$ and $\tilde{\boldsymbol{\phi}} = [0 : 1 : 180]^\circ$, and the true DOAs are located right in the middle of grid points. The additive noise is Gaussian noise, and the array signal-to-noise ratio (SNR) is used in the simulations, defined as $\text{SNR} = 20\log_{10}(\|\mathbf{A}(\boldsymbol{\theta},\boldsymbol{\phi})\mathbf{s}\|_2/\|\mathbf{e}\|_2)$.

The compelling feature of the block-sparse CS is the off-grid DOA compensation, which compensates for the difference between the off-grid true DOAs and the corresponding nearest grid points. This, in turn, produces a sparser solution for block-sparse CS that it utilizes fewer column-blocks than conventional CS [see Figs. 2(a) and 2(b)]. The conventional CS employs more steering vectors to mitigate the grid mismatch and reach the noise floor $\epsilon^{(l_1)}$, which is the basis mismatch problem.[15] Due to the basis mismatch, conventional CS degrades even for high SNR [see Figs. 2(c) and 2(d)].

For the single snapshot (single measurement vector) formulation, the block-sparse CS achieves good DOA estimation and high-resolution, and it is suitable to estimate DOAs from moving sources. The block-sparse CS formulation can be extended to multiple snapshots[4] and sequential processing.[42]

Computations were executed on a 2.4 GHz Intel 8-core i9 processor, and the average CPU times of block-sparse CS and conventional CS were 126 s and 42 s, respectively. The time of block-sparse CS increases by a factor of three; threefold the number of columns in the sensing matrix.

The 2D beamforming accuracy performance is evaluated by ensemble root-mean-square error (RMSE),

$$\text{RMSE} = \sqrt{\text{E}\left[\frac{1}{K}\sum_{k=1}^{K}\left(\left(\hat{\theta}_k-\theta_k\right)^2+\left(\hat{\phi}_k-\phi_k\right)^2\right)\right]}, \tag{18}$$

where $(\hat{\theta}_k, \hat{\phi}_k)$ and (θ_k, ϕ_k) represent the estimated and the true DOAs of the kth source.

We examine scenarios that are the same as in Fig. 2, but grid-intervals ($\{0.5, 1, 2\}^\circ$) and magnitudes ($\text{SNR} = \{0, 5, 10, 15, 20\}$ dB) over 100 trials are considered (see Fig. 3). We set the angular search grids, $\tilde{\boldsymbol{\theta}} = [(-90-0.25) : 0.5 : (90-0.25)]^\circ$ and $\tilde{\boldsymbol{\phi}} = [(0-0.25) : 0.5 : (180-0.25)]^\circ$ for the 0.5° angular grid-interval and $\tilde{\boldsymbol{\theta}} = [(-90-1.5) : 2 : (90-1.5)]^\circ$ and $\tilde{\boldsymbol{\phi}} = [(0-0.5) : 2 : (180-0.5)]^\circ$ for the 2° angular grid-interval, so that the true sources are located right in the middle of grid points for every case. The on-grid case indicates when there is no grid mismatch so the variation of the estimates due to additive noise can be observed. For the on-grid case, angular search grids with $\tilde{\boldsymbol{\theta}} = [-90 : 0.5 : 90]^\circ$

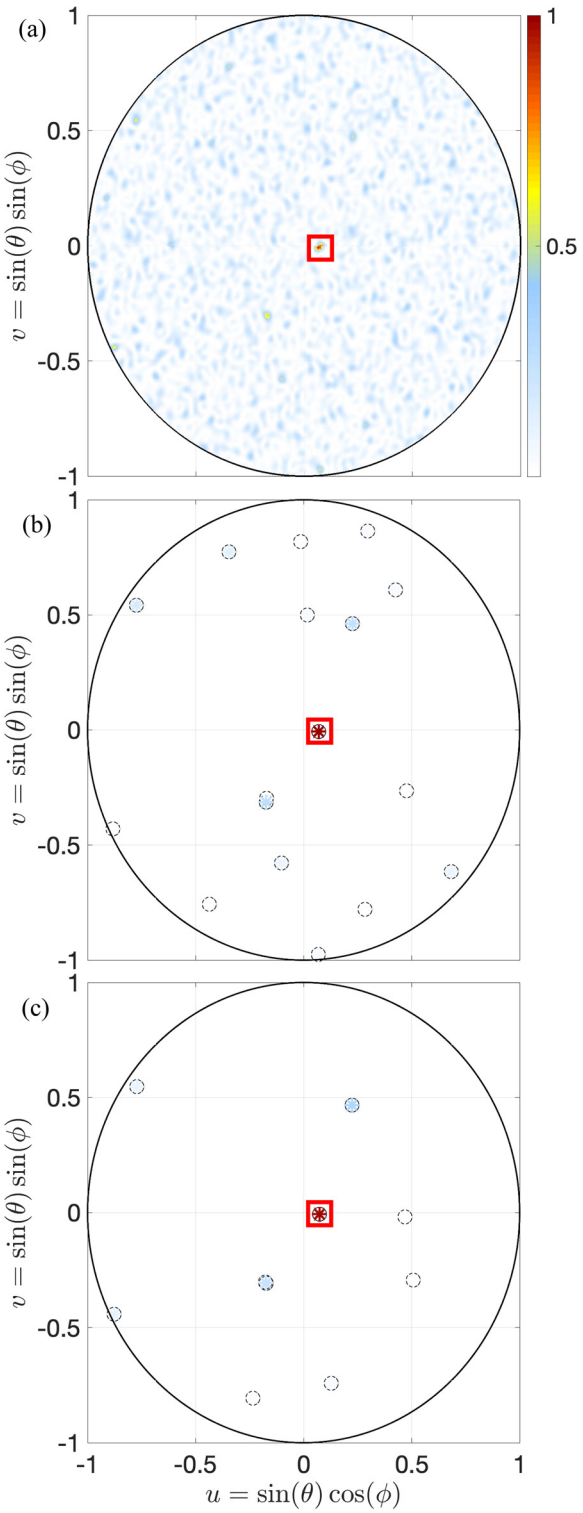

FIG. 4. (Color online) Virtual source experiment results: (a) CBF, (b) conventional CS, and (c) block-sparse CS. Each panel is normalized by its peak value and plotted in power (linear). The estimated DOAs are at $(\boldsymbol{\theta},\boldsymbol{\phi}) = (4.23^\circ, -5.13^\circ)$.

https://doi.org/10.1121/10.0000983

and $\tilde{\phi} = [0 : 0.5 : 180]^\circ$ are used. Block-sparse CS has more accurate DOA estimation than conventional CS with the same grid condition, and block-sparse CS with a coarser grid localizes the sources well compared to conventional CS with a denser grid. Moreover, except for the high SNR region, block-sparse CS with an off-grid case offers similar accuracy to the on-grid case, so that the additive noise takes a dominant portion to RMSE compared to the grid mismatch.

V. EXPERIMENTAL RESULTS

The high-resolution capabilities of block-sparse CS for 2D off-grid DOA estimation and no limitation to a specific array configuration are demonstrated on cavitation tunnel experiment acoustic measurements. The results of the block-sparse CS are compared with those of CBF and conventional CS.

The dataset is from the cavitation tunnel experiment recorded from the array of sensors (B&K 8103) configured with 5 concentric circles of which the radii range from 0.18 to 0.75 m. Each circle consists of 9 hydrophones uniformly separated on the circle, so the array has $M = 45$ sensors (see Fig. 1). For the detailed experimental setup and the characteristics of measured signals with propeller cavitation, see Ref. 39.

Here, we are interested in estimating DOAs from unknown TVC noise source location. To verify the beamforming performance with the experimental setting, a

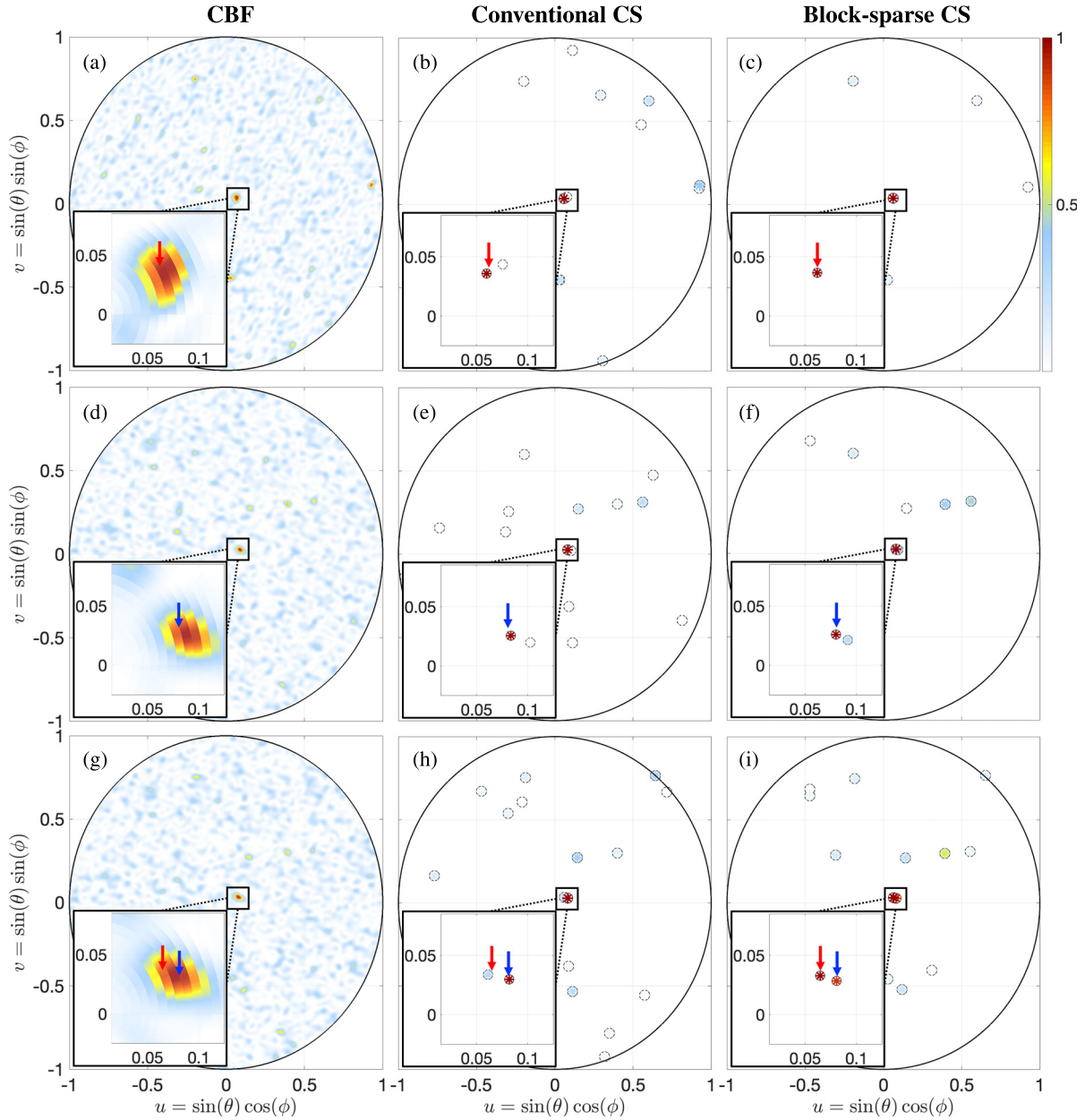

FIG. 5. (Color online) Propeller TVC noise experiment results: (a), (d), (g) CBF; (b), (e), (h) conventional CS; and (c), (f), (i) block-sparse CS. Reference solution DOAs are indicated by red and blue arrows, and the reference solutions are obtained from (c) and (f). Each panel is normalized by its peak value and plotted in power (linear). Two source scenarios are combined [(g)–(i)]: source 1 [(a)–(c)] and source 2 [(d)–(f)].

spherical transducer (ITC-1032) was installed at the end of the propeller shaft offering broadband omni-directional transmitting (0.01−50 kHz), and given the known DOA of the (virtual) source, beamforming is performed. We refer to this experiment as a "virtual source experiment," and the virtual source experiment gives a reference solution to determine the DOAs of TVC noise.

2D beamforming techniques, including CBF, conventional CS, and block-sparse CS, are validated with the virtual source experiment (see Fig. 4). Here, we present a $f = 33.5$ kHz case among a broadband range (0.01−50 kHz). CBF, conventional CS, and block-sparse CS show one dominant source location corresponding to the virtual transducer source location, the same as in Ref. 39. Here, we set the same noise floor ($\epsilon^{(l_1)} = \epsilon = 0.5\|\mathbf{y}\|_2$) for conventional CS and block-sparse CS. Similar to Fig. 2, block-sparse CS shows sparser activate components compared to conventional CS.

Another experiment uses no transducer source; the design propeller was installed and the noise was measured in the occurrence of the propeller TVC, and we refer to this experiment as the "propeller cavitation noise experiment." Here, we present a $f = 30.6$ kHz case with two different snapshots, Figs. 5(a)–5(c) and 5(d)–5(f), respectively, and set the same noise floor ($\epsilon^{(l_1)} = \epsilon = 0.5\|\mathbf{y}\|_2$) for all cases. Incipient propeller TVC noise emits a single significant source near the top center of the propeller,[38–40] and the 2D DOA estimation results show the corresponding DOAs around that position (see Fig. 5).

To verify the high-resolution capability (which can distinguish closely located sources) of block-sparse CS for 2D off-grid DOA estimation, we manipulate the two measurements [$\mathbf{y}_1$ for Figs. 5(a)–5(c) and $\mathbf{y}_2$ for Figs. 5(d)–5(f)] each having a single dominant source but with a slightly different location into one measurement $\mathbf{y}$: $\mathbf{y} = \mathbf{y}_1 + (\|\mathbf{y}_1\|_2/\|\mathbf{y}_2\|_2)\mathbf{y}_2$. Here, we consider the DOAs estimated by block-sparse CS as reference solutions and check whether CBF and conventional CS can distinguish two closely located sources. The noise floor for conventional CS and block-sparse CS is set to $0.5\,\|\mathbf{y}\|_2$, $\epsilon^{(l_1)} = \epsilon = 0.5\,\|\mathbf{y}\|_2$.

CBF merges two sources into one significant peak [see Fig. 5(g)], and conventional CS concentrates power on one source near the two sources [see Fig. 5(h)]; however, block-sparse CS estimates the two sources with equal strength [see Fig. 5(i)].

VI. CONCLUSION

Two-dimensional beamforming for estimating both DOAs in azimuth and elevation is formulated as a sparse signal reconstruction problem and solved efficiently using CS with a sparsity constraint. To estimate off-grid DOAs, which do not coincide with the angular search grid, we suggested the off-grid DOA estimation scheme. The off-grid DOA estimation is achieved by jointly processing the terms, including the discretized angular grid and the offset terms for off-grid azimuth and off-grid elevation, in the concept of a block and solved using CS with a block-sparsity constraint. Also, the presented model is not limited to a specific array configuration, which can fit in with realistic scenarios.

Numerical simulations show that the proposed method provides improved estimation accuracy. The real data example indicates that the algorithm provides a high-resolution 2D beamforming performance and can distinguish closely located DOAs that CBF and conventional CS cannot.

ACKNOWLEDGMENTS

This research was supported by the Office of Naval Research, Grant No. N00014-18-1-2118, and the Agency for Defense Development in the Republic of Korea under Contract No. UD190005DD.

[1]D. L. Donoho, "Compressed sensing," IEEE Trans. Inf. Theory **52**(4), 1289–1306 (2006).
[2]D. Malioutov, M. Cetin, and A. S. Willsky, "A sparse signal reconstruction perspective for source localization with sensor arrays," IEEE Trans. Signal Process. **53**(8), 3010–3022 (2005).
[3]A. Xenaki, P. Gerstoft, and K. Mosegaard, "Compressive beamforming," J. Acoust. Soc. Am. **136**(1), 260–271 (2014).
[4]P. Gerstoft, A. Xenaki, and C. F. Mecklenbräuker, "Multiple and single snapshot compressive beamforming," J. Acoust. Soc. Am. **138**(4), 2003–2014 (2015).
[5]P. Gerstoft, C. F. Mecklenbräuker, W. Seong, and M. Bianco, "Introduction to compressive sensing in acoustics," J. Acoust. Soc. Am. **143**, 3731–3736 (2018).
[6]A. Drémeau, F. Le Courtois, and J. Bonnel, "Reconstruction of dispersion curves in the frequency-wavenumber domain using compressed sensing on a random array," IEEE J. Ocean. Eng. **42**(4), 914–922 (2017).
[7]F. Le Courtois and J. Bonnel, "Compressed sensing for wideband wavenumber tracking in dispersive shallow water," J. Acoust. Soc. Am. **138**(2), 575–583 (2015).
[8]M. Bianco and P. Gerstoft, "Compressive acoustic sound speed profile estimation," J. Acoust. Soc. Am. **139**(3), EL90–EL94 (2016).
[9]K. L. Gemba, W. S. Hodgkiss, and P. Gerstoft, "Adaptive and compressive matched field processing," J. Acoust. Soc. Am. **141**(1), 92–103 (2017).
[10]Y. Park, W. Seong, and Y. Choo, "Compressive time delay estimation off the grid," J. Acoust. Soc. Am. **141**(6), EL585–EL591 (2017).
[11]Y. Park, P. Gerstoft, and W. Seong, "Grid-free compressive mode extraction," J. Acoust. Soc. Am. **145**(3), 1427–1442 (2019).
[12]A. Xenaki and Y. Pailhas, "Compressive synthetic aperture sonar imaging with distributed optimization," J. Acoust. Soc. Am. **146**(3), 1839–1850 (2019).
[13]S. Nannuru, A. Koochakzadeh, K. L. Gemba, P. Pal, and P. Gerstoft, "Sparse Bayesian learning for beamforming using sparse linear arrays," J. Acoust. Soc. Am. **144**(5), 2719–2729 (2018).
[14]S. Nannuru, K. L. Gemba, P. Gerstoft, W. S. Hodgkiss, and C. F. Mecklenbräuker, "Sparse Bayesian learning with multiple dictionaries," Signal Proc. **159**, 159–170 (2019).
[15]A. Xenaki and P. Gerstoft, "Grid-free compressive beamforming," J. Acoust. Soc. Am. **137**(4), 1923–1935 (2015).
[16]Y. Park, Y. Choo, and W. Seong, "Multiple snapshot grid free compressive beamforming," J. Acoust. Soc. Am. **143**(6), 3849–3859 (2018).
[17]Z. Yang, L. Xie, and C. Zhang, "Off-grid direction of arrival estimation using sparse Bayesian inference," IEEE Trans. Signal Process. **61**(1), 38–43 (2012).
[18]C. P. Mathews and M. D. Zoltowski, "Eigenstructure techniques for 2-D angle estimation with uniform circular arrays," IEEE Trans. Signal Process. **42**(9), 2395–2407 (1994).
[19]M. D. Zoltowski, M. Haardt, and C. P. Mathews, "Closed-form 2-D angle estimation with rectangular arrays in element space or beamspace via unitary esprit," IEEE Trans. Signal Process. **44**(2), 316–328 (1996).

[20]A. M. Elbir and T. E. Tuncer, "2-D DOA and mutual coupling coefficient estimation for arbitrary array structures with single and multiple snapshots," Digit. Signal Process. **54**, 75–86 (2016).
[21]J. Shi, G. Hu, X. Zhang, F. Sun, and H. Zhou, "Sparsity-based two-dimensional DOA estimation for coprime array: From sum–difference coarray viewpoint," IEEE Trans. Signal Process. **65**(21), 5591–5604 (2017).
[22]S. Nannuru and P. Gerstoft, "2D beamforming on sparse arrays with sparse Bayesian learning," in *Proceeding of the IEEE International Conference of Acoustics, Speech, and Signal Processing (ICASSP)*, Brighton, UK (May 12–17, 2019), pp. 4355–4359.
[23]Y. Chi and Y. Chen, "Compressive two-dimensional harmonic retrieval via atomic norm minimization," IEEE Trans. Signal Process. **63**(4), 1030–1042 (2014).
[24]Z. Yang, L. Xie, and P. Stoica, "Vandermonde decomposition of multilevel toeplitz matrices with application to multidimensional super-resolution," IEEE Trans. Inf. Theory **62**(6), 3685–3701 (2016).
[25]Y. Yang, Z. Chu, Z. Xu, and G. Ping, "Two-dimensional grid-free compressive beamforming," J. Acoust. Soc. Am. **142**(2), 618–629 (2017).
[26]J. Li, Y. Li, and X. Zhang, "Two-dimensional off-grid DOA estimation using unfolded parallel coprime array," IEEE Commun. Lett. **22**(12), 2495–2498 (2018).
[27]F. F. Shen, Y. M. Liu, G. H. Zhao, X. Y. Chen, and X. P. Li, "Sparsity-based off-grid DOA estimation with uniform rectangular arrays," IEEE Sens. J. **18**(8), 3384–3390 (2018).
[28]Y. C. Eldar, P. Kuppinger, and H. Bolcskei, "Block-sparse signals: Uncertainty relations and efficient recovery," IEEE Trans. Signal Process. **58**(6), 3042–3054 (2010).
[29]Z. Zhang and B. D. Rao, "Extension of SBL algorithms for the recovery of block sparse signals with intra-block correlation," IEEE Trans. Signal Process. **61**(8), 2009–2015 (2013).
[30]H. L. Van Trees, *Optimum Array Processing (Detection, Estimation, and Modulation Theory*, *Part IV)* (Wiley-Interscience, New York, 2002), Chaps. 1–10.
[31]J. Choi and S. A. Kinnas, "Numerical model of cavitating propeller inside of a tunnel," J. Fluids Eng. **121**(2), 297–304 (1999).
[32]J. Bosschers, G. Vaz, A. Starke, and E. van Wijngaarden, "Computational analysis of propeller sheet cavitation and propeller-ship interaction," in *Proceedings of RINA Conference MARINE CFD2008*, Southampton, UK (March 26–27, 2008), pp. 26–27.
[33]J. Lee, J. Jung, K. Lee, J. Han, H. Park, and J. Seo, "Experimental estimation of a scaling exponent for tip vortex cavitation via its inception test in full- and model-ship," J. Hydrodynam. B **24**(5), 658–667 (2012).
[34]G. Tani, M. Viviani, E. Armelloni, and M. Nataletti, "Cavitation tunnel acoustic characterisation and application to model propeller radiated noise measurements at different functioning conditions," Proc. Inst. Mech. Eng. M **230**(2), 250–266 (2016).
[35]C. Park, H. Seol, K. Kim, and W. Seong, "A study on propeller noise source localization in a cavitation tunnel," Ocean Eng. **36**(9–10), 754–762 (2009).
[36]J. Lee, J. Han, H. Park, and J. Seo, "Application of signal processing techniques to the detection of tip vortex cavitation noise in marine propeller," J. Hydrodynam. B **25**(3), 440–449 (2013).
[37]K. Lee, J. Lee, D. Kim, K. Kim, and W. Seong, "Propeller sheet cavitation noise source modeling and inversion," J. Sound Vib. **333**(5), 1356–1368 (2014).
[38]D. Kim, W. Seong, Y. Choo, and J. Lee, "Localization of incipient tip vortex cavitation using ray based matched field inversion method," J. Sound Vib. **354**, 34–46 (2015).
[39]C. Park, G. Kim, Y. Park, K. Lee, and W. Seong, "Noise localization method for model tests in a large cavitation tunnel using a hydrophone array," Remote Sens. **8**(3), 195–218 (2016).
[40]Y. Choo and W. Seong, "Compressive spherical beamforming for localization of incipient tip vortex cavitation," J. Acoust. Soc. Am. **140**(6), 4085–4090 (2016).
[41]M. Grant and S. Boyd, "CVX: Matlab software for disciplined convex programming, version 2.1," (2014), available at http://cvxr.com/cvx (Last viewed October 1, 2019).
[42]C. F. Mecklenbräuker, P. Gerstoft, A. Panahi, and M. Viberg, "A sparse signal reconstruction perspective for source localization with sensor arrays," IEEE Trans. Signal Process. **61**(24), 6344–6354 (2013).